environmental microbiology

Environmental Microbiology (2015) doi:10.1111/1462-2920.13054

High-resolution analysis of the *m*-xylene/toluene biodegradation subtranscriptome of *Pseudomonas putida* mt-2

Juhyun Kim, Danilo Pérez-Pantoja,[†] Rafael Silva-Rocha,[‡] Juan Carlos Oliveros and Víctor de Lorenzo*

Systems Biology Program, Centro Nacional de Biotecnologia-CSIC, Campus de Cantoblanco, Madrid, Spain.

Summary

Pseudomonas putida **mt-2 metabolizes *m*-xylene and other aromatic compounds through the enzymes encoded by the *xyl* operons of the TOL plasmid pWW0 along with other chromosomally encoded activities. Tiling arrays of densely overlapping oligonucleotides were designed to cover every gene involved in this process, allowing dissection of operon structures and exposing the interplay of plasmid and chromosomal functions. All *xyl* sequences were transcribed in response to aromatic substrates and the 3′-termini of both *upper* and *lower* mRNA operons extended beyond their coding regions, i.e. the 3′-end of the *lower* operon mRNA penetrated into the convergent *xylS* regulatory gene. Furthermore, *xylR* mRNA for the master *m*-xylene responsive regulator of the system was decreased by aromatic substrates, while the cognate *upper* operon mRNA was evenly stable throughout its full length. RNA sequencing confirmed these data at a single nucleotide level and refined the formerly misannotated *xylL* sequence. The chromosomal *ortho* route for degradation of benzoate (the *ben*, *cat* clusters and some *pca* genes) was activated by this aromatic, but not by the TOL substrates, toluene or *m*-xylene. We advocate this scenario as a testbed of natural retroactivity between a pre-existing metabolic network and a new biochemical pathway implanted through gene transfer.**

Received 2 June, 2015; revised 30 August, 2015; accepted 12 September, 2015. *For correspondence. E-mail vdlorenzo@cnb.csic.es; Tel. (+34-91) 585 45 36; Fax (+34-91) 585 45 06. Present addresses: [†]Departamento de Bioquímica y Biología Molecular, Facultad de Ciencias Biológicas, Universidad de Concepción, Chile; [‡]Department of Cell and Molecular Biology, Ribeirão Preto Medical School, Universidade de São Paulo 14049-900, Brazil.

Introduction

Pseudomonas putida mt-2, host of the TOL plasmid pWW0, is able to assimilate *m*-xylene or toluene through a set of enzymes encoded by the catabolic plasmid (Worsey and Williams, 1975; Assinder and Williams, 1990; Marques *et al*., 1999). Two plasmid-encoded operons account for the entire metabolic process that leads to biodegradation of such aromatic substrates (Fig. 1). The *upper* operon determines enzymes that convert *m*-xylene or toluene into 3-methylbenzoate (i.e. 3MBz) or benzoate, respectively, and the *lower* operon enzymes catalysing the conversion of 3MBz into 3-methylcatechol or benzoate into catechol and its ensuing *meta* ring cleavage, which ultimately leads to intermediates of the TCA cycle (Assinder and Williams, 1990; Ramos *et al*., 1997). At the same time, benzoate is also degraded via the chromosomally encoded *ortho* pathway genes, i.e. *ben*, *cat* and *pca* (Harwood and Parales, 1996; Jimenez *et al*., 2002). The TOL plasmid-encoded transcriptional factors called XylR and XylS control the expression of the corresponding *upper* and *lower* operons. The principal regulatory interactions between metabolic and regulatory components of the TOL network are sketched in Fig. 1. In addition to these plasmid-encoded regulators and promoters, a number of host factors influence expression of the TOL functions, e.g. the integration host factor and the HU nucleoid-associated proteins (Perez-Martin and de Lorenzo, 1995) and the TurA and PprA products (Rescalli *et al*., 2004; Vitale *et al*., 2008). Besides, the TOL system is subject to various catabolite repression and physiological control checks (Velazquez *et al*., 2004; Aranda-Olmedo *et al*., 2005; Moreno *et al*., 2010). In this scenario, pWW0-borne proteins and host native regulators and small molecules interact to shape a complex metabolic and transcriptional circuit that has recently been reviewed (Silva-Rocha *et al*., 2011a) and (at least partially) modelled (Silva-Rocha *et al*., 2011b). Specific nodes of such a network have been studied in extraordinary molecular detail (Koutinas *et al*., 2010; Silva-Rocha *et al*., 2011a), and even more regulatory devices are likely to appear. The reason for the apparently unnecessary intricacy of the genetic circuitry found in the TOL system is still unexplained (Silva-Rocha *et al*., 2011b).

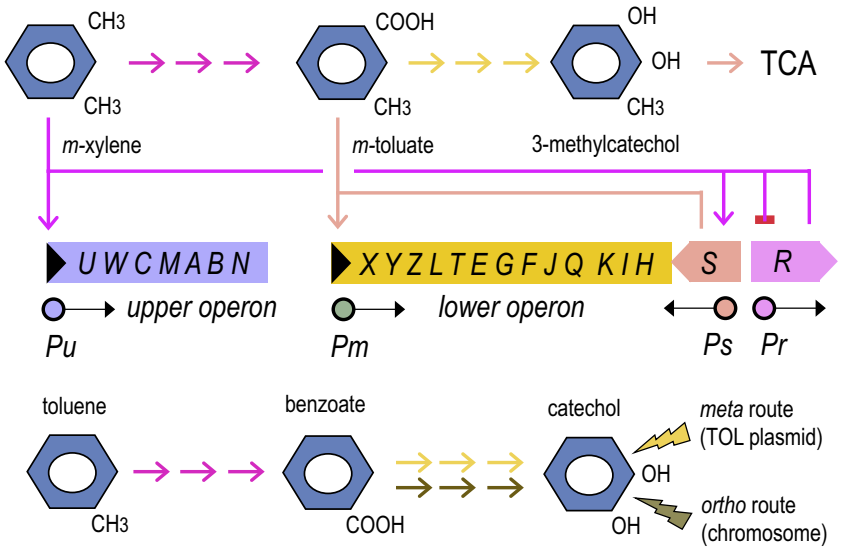

Fig. 1. The TOL regulatory and metabolic network for *m*-xylene and toluene biodegradation borne by the catabolic enzymes in the TOL plasmid. The top part of the figure shows the principal actors of the process. In the presence of *m*-xylene or toluene, XylR (expressed from *Pr*) activates both the σ^{54}-dependent promoters *Pu* (which transcribes the *upper* pathway operon) and *Ps*, which drives expression of *xylS* (Perez-Martin and de Lorenzo, 1995; Bertoni *et al.*, 1998). Since the *Pr* promoter overlaps the XylR binding sites of the divergent *Ps* promoter, XylR expression is negatively auto-regulated (Bertoni *et al.*, 1998). In turn, the XylS protein activates *Pm*, the promoter of the *lower* operon (Bertoni *et al.*, 1998; Marques *et al.*, 1999; Dominguez-Cuevas *et al.*, 2008; 2010). *Pr*, *Ps*, *Pu* and *Pm* promoters are indicated in front of each cognate gene or operon. By default, XylS is expressed at a low level but its transcription is enhanced by XylR in the presence of *m*-xylene. The bottom part of the figure signifies that the benzoate produced by partial metabolism of toluene can be channelled through either the *meta* ring-cleavage pathway encoded by the lower TOL operon or through the *ortho*-ring-fission route encoded in the host's chromosome.

One approach to addressing the exaggerated complexity of the TOL network is to examine the regulatory behaviour of the entire system rather than its parts. Velazquez and colleagues (2005) and Dominguez-Cuevas and colleagues (2006) first documented the genome-wide transcriptional response of *P. putida* mt-2 when cells faced various aromatic compounds – whether they were TOL substrates or not. While these studies were instrumental in verifying the layout of the regulatory circuit proposed earlier on the basis of one-at-a-time reporter fusions to the TOL promoters (Hugouvieux-Cotte-Pattat *et al.*, 1990; Marques *et al.*, 1994), the technology of the time was insufficient to examine key aspects of the *m*-xylene sub-transcriptome, e.g. the fine structure of the TOL operons, the regulatory cross-talk of plasmid and host metabolic genes, and the action of post-transcriptional RNA-based regulation devices.

To overcome this impasse and generate a high-definition expression profile of such catabolic genes, we have designed and exploited in this work a tiling array (Selinger *et al.*, 2000; Guell *et al.*, 2009) that spans 14 704 base pairs (bp) of DNA, including the two strands of the corresponding *xyl* genes of the TOL system in its entirety, as well as the chromosomal *ortho* pathway genes involving *ben*, *cat* and *pca* sequences. Experiments with this array were complemented and validated with deep RNA sequencing (RNA-seq; Passalacqua *et al.*, 2009; Toledo-Arana *et al.*, 2009; Yoder-Himes *et al.*, 2009; Kim *et al.*, 2013) that gave further insights into the regulatory components of the TOL catabolic system - in particular the interplay between the pWW0-encoded and the chromosomally encoded pathways for metabolism of benzoate in *P. putida* mt-2.

Results and Discussion

Benchmarking tiling arrays and RNA-seq for visualizing the structure of xyl transcripts

As the starting point of this work, the structure and abundance of the transcripts that originate in each of the four promoters (*Pu*, *Pm*, *Pr*, *Ps*) in front of the *xyl* genes of the TOL plasmid (Fig. 1) were examined by combining tiling array technology and deep RNA-seq. In one case, a custom tiling microarray was designed to contain probes corresponding to the complete *xyl* operons of the TOL plasmid, as well as chromosome clusters covering both branches of β-ketoadipate pathway comprising the *fcs* cluster, the *pca* genes, the *ben* genes and the *cat* genes. Note that tiling arrays are strand specific, what allows gaining details on transcript structure that may not be evident with other techniques (Huber *et al.*, 2006; Miyakoshi *et al.*, 2009; Mader *et al.*, 2011). Once we had such arrays in hand, *P. putida* mt-2 strain was cultured to early exponential growth phase (OD_{600} ~ 0.3) in succinate-

supplemented minimal medium and then exposed to saturating vapours of a 1:2 dilution of *m*-xylene (the canonical substrate of the TOL network) in dibutyl phthalate. Two hours later, total RNAs were isolated and the cDNAs synthesized were used for hybridization to the tiling array chip. In addition to these conditions, we also prepared a second control sample by culturing the cells in succinate as the sole carbon source and then let them run out of carbon for an extended period of time (96 h). Such prolonged carbon starvation is predicted to empty cells of the mRNAs of interest, making this reference instrumental as a baseline for comparisons (Guell *et al*., 2009). Expression intensity was normalized by comparing either cells grown in succinate to those in succinate plus *m*-xylene or to the alternative C-runout condition. It should be noted in any case that succinate does not interfere with *xyl* gene expression (Holtel *et al*., 1994; Cases *et al*., 1999).

Consistent with previous observations using DNA array technology (Velazquez *et al*., 2005), results from the tiling array showed that all TOL *upper* and *lower* pathway genes and the *xylS* gene were highly expressed in response to *m*-xylene, whereas the *xylR* gene appeared to be downregulated in the same conditions (Fig. 2A). To determine the relative gene expression level, the tiling array data were normalized to the RNAs from succinate-cultured cells (Fig. 2A) or to cells starved for 96 h (Fig. 2B). The overall expression pattern was the same regardless of the reference used (Fig. 2). Yet, absolute differences were more pronounced when data were normalized in respect to the starved cells as compared with those of *m*-xylene-cultured cells versus succinate-grown cells (Fig. 2). This was probably caused by a residual level of transcription for the *xyl* genes in succinate even in the absence of the aromatic inducer, particularly in the case of the *lower* TOL operon. In addition, when using succinate only as a control, transcription intensity was not evenly distributed through the genes of the *lower* pathway. Under the same conditions (i.e. using succinate-cultured cells as control), transcription of the *upper* pathway genes was uniform throughout the entire length of the cognate DNA sequence (Fig. 2A). By contrast, the transcriptional profiles of both the *upper* and the *lower* operons were evenly distributed when the RNA from C-runout cells was used for normalization (Fig. 2B).

In sum, these data accredit that the *lower* pathway genes are expressed to a low but detectable level in succinate-amended minimal medium in the absence of inducers or substrates to be. In view of these results, we adopted the C-runout condition as the default reference for subsequent analyses (Fig. 2B, lower panel), as it seems to faithfully reflect the no-induction baseline of the *upper* and *lower* operons. To verify this, we revisited the net *m*-xylene-dependent expression profile of *xyl* genes with deep RNA-seq (Fig. 3). To this end, the cDNA libraries from RNA extracted from the bacteria under examination cells were sequenced using the Illumina Genome Analyzer IIx system, and the reads were mapped to the pWW0 plasmid sequence (and also the *P. putida* KT2440 chromosome, see below). The alignment to the *upper* and *lower* pathway genes of the TOL plasmid was visualized

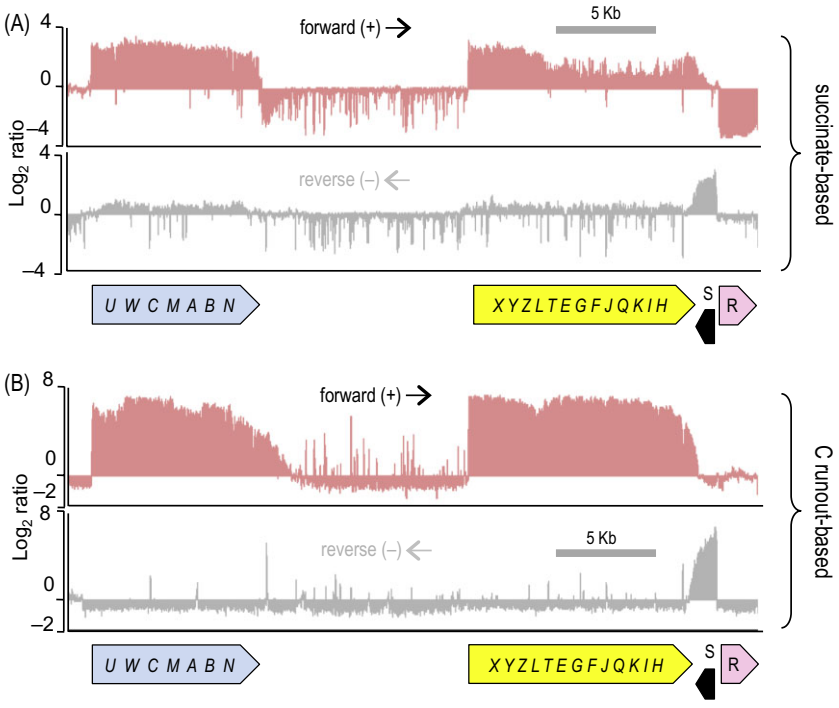

Fig. 2. High-density tiling array-based transcriptome profile of TOL *xyl* genes in *P. putida* mt-2.
A. Relative gene expression intensity of pWW0-encoded *xyl* genes in *P. putida* mt-2 grown in succinate and treated or not with saturating vapours of *m*-xylene, using cells grown on succinate only as reference conditions.
B. Same, but using as a reference the mRNA from *P. putida* mt-2 cells grown in succinate and let run out of carbon upon prolonged culturing for 96 h. Red signals, forward transcription; gray signals, reverse transcription. The DNA segments spanning the *xyl* genes are indicated with arrowed boxes: *upper* (light blue) and *lower* (yellow). The black box indicates the *xylS* gene. IGB software was used for visualization.

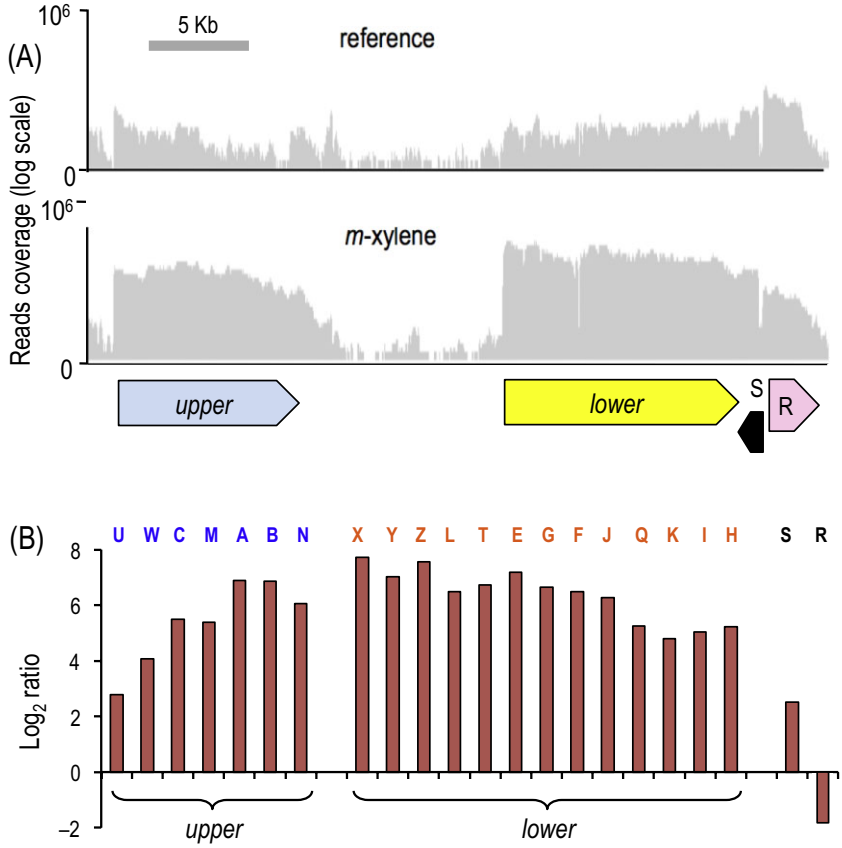

Fig. 3. RNA deep sequencing-based transcriptome profile of TOL *xyl* genes in *P. putida mt-2*.
A. Total numbers of cDNA reads are annotated responding to the *xyl* genes in RNA isolated from the C-runout reference (top panel) or *m*-xylene-exposed cells (bottom panel). IGV software was used for visualization.
B. Normalization of transcription intensity for the *xyl* genes, comparing *m*-xylene-cultured and C-runout conditions. Arrowed boxes: *upper* (light blue), *lower* (yellow), *xylS* (black), *xylR* (pink).

using the IGV (integrated genome viewer) software (Thorvaldsdottir *et al*., 2012) as shown in Fig. 3A, and the transcription activity was normalized (Fig. 3B) by trimmed mean of M values (TMM; Robinson and Oshlack, 2010). Although the expression intensity level cannot be compared quantitatively with the tiling array data, the transcription profiles from RNA-seq results were fully consistent with the array-based expression pattern (e.g. compare Figs 2 and 3). The mutually complementary tiling arrays and deep RNA-seq were thereafter adopted as a reliable approach to examine the whole *P. putida* mt-2 subtranscriptome involved in biodegradation of aromatic substrates.

Definition of operon structure of TOL genes, novel transcriptional units and correction of gene annotation

Improved resolution by high-density tiling microarrays and deep RNA-seq provides insights into genomic elements, e.g. discovery of new genes, definition of untranslated regions and operon structure (Sorek and Cossart, 2010). We thus proceeded to examine the structure of the TOL operons as they appear when cells are exposed to *m*-xylene. Using these methods, we found some new transcriptional features in TOL *xyl* genes. The first novelty was the presence of a previously unreported and apparently separate ~1000 bp-long transcription unit downstream of the *xylN* gene (Fig. 2B; Fig. S1). Consistent with the tiling array data, this transcription unit was also observed with the RNA-seq, as reads mapped to the same region at a high rate (Fig. 3A). This mRNA extension unit overlaps in part with an open reading frame of unknown function (*orf*126) that is also found in other TOL plasmids such as pD2RT, pDK1 and pWW53. *orf*126 is adjacent to the downstream end of the *upper* operon and transcription from *Pu* runs through its complete sequence (see Fig. S1 for a blow-up of the region). However, the separate transcript occurs regardless of growth conditions (Fig. 4) and might be therefore constitutively expressed – or induced by an unknown metabolic effector.

Apart of this trait, both transcriptomic approaches confirmed the already recognized operon structures of the *xyl* genes (Harayama *et al*., 1984; 1989; Marques *et al*., 1993; Williams *et al*., 1997). Furthermore, the relatively even signals through the whole length of both the *upper* and the *lower* operons suggested that the bulk of the *xyl* transcripts generated under the conditions tested was long, polycistronic mRNAs, with little indication of differential stability, processing or additional internal promoters. Still, under some conditions (Fig. 4), we could detect an apparent boundary between the *xylXYZL* portion of the *meta* pathway transcripts and the rest of the operon, a

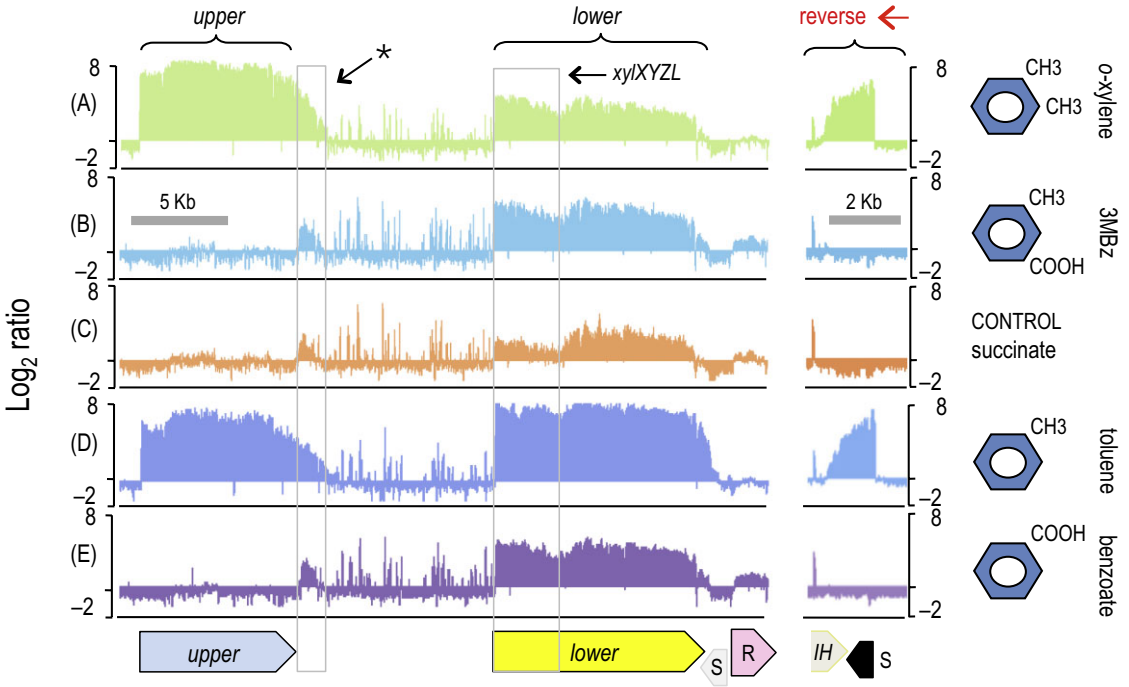

Fig. 4. Transcriptome profiles of core TOL catabolic system of *P. putida* mt-2 responding to related aromatic compounds using a high-density tiling array. Expression of the *xyl* genes was examined in cells exposed to (A) *o*-xylene, (B) 3MBz, (D) toluene and (E) benzoate respectively. The middle panel (C) is a control with non-induced succinate-grown cells. Signals are normalized in respect to the C-runout condition. Y-axis, Log_2 signal ratio. The transcript identified downstream of the end of the *upper* operon (after the 3′ end of *xylN*) is indicated with a cage (*). The sequences corresponding to the *xylXYZL* genes are indicated as well. Arrowed boxes: *upper* (light blue), *lower* (yellow), *xylS* (black), *xylR* (pink). The reverse transcription of the *xylIH/xylS* segment is shown to the right of the panels.

circumstance that has been reported before (Harayama and Rekik, 1990; Marques *et al.*, 1993). However, this discontinuity disappeared when the system was fully induced with *m*-xylene (Fig. 2B). We also found that the *xylL* sequence present in the *P. putida* mt-2 strain under examination had a manifest divergence in respect to the corresponding data in the literature (Greated *et al.*, 2002). From the RNA-seq results, no sequencing read could be aligned to a 36 bp segment of the *xylL* gene annotated in NCBI (GenBank: AJ344068.1; Fig. S2). To test whether this was caused by a technical error in the RNA-seq or the problem stems from the gene sequence proper, we cloned the partial *xylL* gene of our *P. putida* mt-2 clone and analysed the DNA of that region. This revealed that the section between coordinates 52320–52355 in the plasmid was absent in our template DNA (Fig. S2). Since the product of *xylL* is necessary for processing *cis*-dihydrodiols generated during dioxygenation of 3MBz (Voss *et al.*, 1990) and our strain grows perfectly well on *m*-xylene and 3MBz, it is unlikely that the loss of this 36 bp sequence could be attributed to a spontaneous deletion in the laboratory. Moreover, all other annotated *xylL* orthologues that are found in databases lack also the segment missing in our pWW0 variant (not shown).

Overlapping transcription between the 3′ ends of xylS and the lower operon gene

As mentioned above, tiling arrays expose details on transcript structure that may go unnoticed with bulk RNA-seq. One intriguing feature of the regulatory architecture of the TOL network is that the gene encoding the regulatory protein XylR is located in the pWW0 frame adjacent to one target promoter (*Ps*) but distal to the other (*Pu*). In contrast, the second regulatory factor (*xylS*) is away from the promoter it controls (*Pm*), but it is located adjacent and opposite to the end of the terminus of the *meta* operon whose transcription is driven by *Pm* (Fig. 1). Inspection of the convergent strand-specific signals originated at the 3′ termini of the *meta* operon and the *xylS* gene (Figs 2B and 5A) revealed that they both overlap by at least 350 nt. Most of the overlap occurs in non-coding regions, but the shared segment reaches out short portions of either 3′-end gene sequences. Since such a confluence could have a regulatory value, we verified this state of affairs with Northern blot analysis of transcript production at this overlapping region with strand-specific RNA probes prepared with the *in vitro* transcription method described in *Experimental procedures*. These

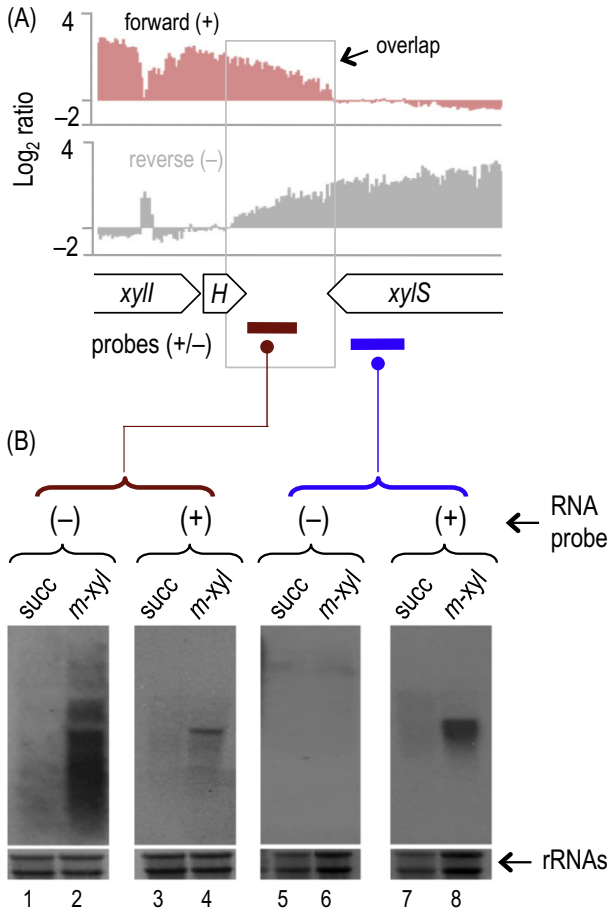

Fig. 5. Northern blot analysis of the 3′ overlapping mRNAs downstream of *xylH* and *xylS*.
A. Organization of the intergenic *xylH* and *xylS* regions and extent of their overlaps. The segments covered by the RNA probes to test direct and reverse transcription at each location are indicated: non-coding, red; intragenic region of *xylS*, blue.
B. Northern blots of *P. putida* mt-2 mRNA extracted from cultures from either succinate only (succ) or succinate plus *m*-xylene (*m*-xyl) hybridized with the ^{32}P-RNA probes indicated in each case. The lower panels show intensities of rRNAs used as controls.

probes were designed for either strand of the two non-coding sequences between the *xylS* and the end of the *lower* operon region. Both probes were directly hybridized with total RNAs from *m*-xylene-exposed cells (Fig. 5A, red line). Several signals originated in the non-coding regions were detected by the antisense probe, indicating that they were indeed transcribed (in contrast with the more modest signals for the sense probe; Fig. 5B). When an internal probe for *xylS* was used (Fig. 5B, blue line), only the sense probe delivered a signal. This meant that the untranslated 3′ ends of the *xylH* and *xylS* transcripts could reach out each other well, thereby raising the question of whether such a convergent transcription of the region of confluence results in a pairing structure between sense and antisense transcripts that could have a regulatory effect (Thomason and Storz, 2010). To explore this possibility, we constructed an artificial antisense *xylS* expression system as sketched in Fig. 6A. The business part of plasmid pSEVA224-XS consists of a DNA segment spanning *xylS* and its extended 3′-end bound upstream by the native *Ps* promoter of *xylS* but added downstream with a reverse IPTG-inducible *Ptrc* promoter. This plasmid was introduced into the *P. putida* strain harbouring the *Pm* promoter fused to a bi-cistronic *gfp-lacZ* reporter system (Silva-Rocha and de Lorenzo, 2012). Should the untranslated mRNA downstream of the *xylH* gene (expressed from *Ptrc* in plasmid pSEVA224-XS) influence expression of *xylS*, the prediction is that we should see an effect on the activity of the *Pm–GFP* fusion of the host strain. To test this possibility, we inspected GFP levels in single cells with flow cytometry. As shown in Fig. 6B, *Pm* activity and distribution in individual bacteria was impervious to the increase of anti-sense RNA, as GFP expression followed in all cases a graded pattern with no changes in activity or expression noise (Fig. 6B). These results indicated that overlapping transcripts downstream of *xylS* lack any gross influence on the behaviour of the TOL regulatory network.

Response of the TOL network to gratuitous induction and to 3MBz

To complete the picture of the response of the TOL network to its canonical substrate, *m*-xylene, we examined the expression pattern of the corresponding gene clusters under two additional conditions with tiling arrays as before. In one case, we exposed the cells to *o*-xylene. This is a non-metabolizable but strong effector of the master XylR regulator that should directly trigger the targets of this transcription factor (i.e. the *Ps* and the *Pu* promoters of the TOL system; Fig. 1). Indirectly, the *Pm* promoter is expected to be activated in the presence of *o*-xylene also due to the regulatory effect of overproduced XylS even in the absence of its metabolic effector (the metabolic intermediate 3MBz). Figure 4A shows the expression profile of each portion of the TOL segments of pWW0 plasmid in response to *o*-xylene. This gratuitous XylR effector triggered the expression of the *upper* operon to similar or even higher levels than the genuine pathway substrate, *m*-xylene (compare Fig. 4A with Fig. 2B). The same held true for the XylR-activated expression of the *xylS* gene. In contrast, the volume of transcripts of the *meta* operon originated in the *Pm* promoter was significantly less with *o*-xylene than with *m*-xylene. This made sense, as activation of *Pm* under these conditions stems only from overproduction of XylS, thereby lacking the cascade effect caused by 3MBz when it is produced out of metabolism of *m*-xylene (Fig. 1). Regardless of differences in levels, comparison of the mRNA profiles of the *xyl* genes induced with either *m*-xylene or *o*-xylene

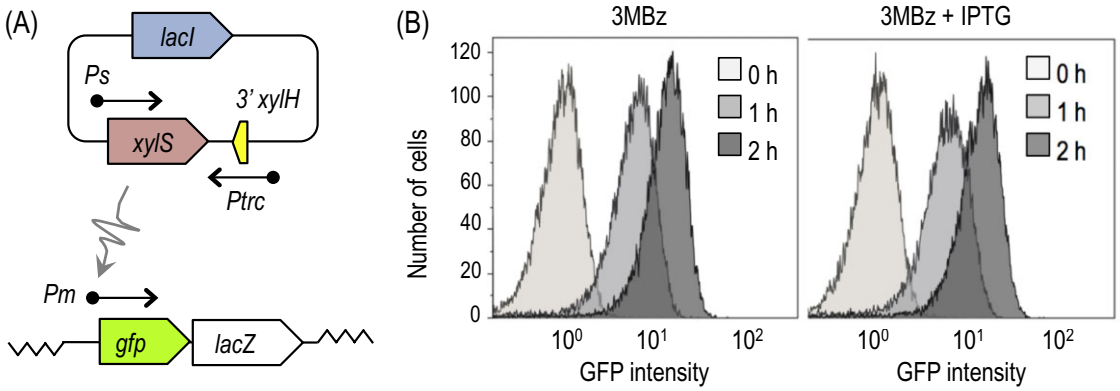

Fig. 6. Assay for the effect of confluent *xylH/xylS* transcription on the *Pm* promoter.
A. Regulatory elements engineered in reporter strain *P. putida* MEG3D (*Pm* → *GFP-lacZ*/pSEVA224-XS).
B. Flow cytometry analysis for GFP activity. The reporter strain was cultured in succinate-amended M9 minimal medium overnight. Cells (diluted 100-fold) were inoculated on the same medium and cultured until early exponential growth phase (OD_{600} ~0.2). At this time, cultures were divided into three conditions for control, 3MBz (5 mM) and 3MBz plus IPTG (1 mM). After adding these substrates, the cells were cultured and harvested after 1 or 2 h. For each sample, 1.5×10^4 cells were analysed by flow cytometry.

indicated the organization and relative stability of segments throughout the mRNAs to be virtually identical. This suggested that there is little or no connection between expression of these catabolic genes and actual catabolic activity and that neither the substrate nor its metabolic intermediates influence production of full-length mRNAs through riboswitches or other regulatory devices.

The second condition tested involved addition of 3MBz to *P. putida* mt-2 cultures. As mentioned above, this aromatic intermediate is produced metabolically upon the action of the *upper* pathway gene products on *m*-xylene, but can also be added exogenously for separate induction of the *lower* TOL operon (Gonzalez-Perez *et al*., 2004). Figure 4B shows the result of such an induction experiment. While the *upper* TOL pathway remained silent and expression of the *xylS* was not affected, transcription of the lower TOL pathway was upregulated but to a much lower level than the same in cells induced with *m*-xylene (compare Fig. 4B with Fig. 2B). These data were consistent with the current regulatory model of the TOL network, in which the *Ps* promoter is in reality composed of two tandem promoters (Gallegos *et al*., 1996): one low constitutive (*Ps2*) and one inducible at high levels by *m*-xylene/XylR (*Ps1*). When 3MBz is added to the cells, only low levels of XylS are available to activate the expression of the *lower* pathway. This thus happens to a limited extent, as the cognate regulatory node lacks in this case the amplifying effect of overproducing XylS.

Transcriptomic fingerprint of toluene catabolism through the TOL pathway

The data examined above concern exclusively the transcriptomic background of degradation of *m*-xylene or 3MBz, the canonical substrates of the TOL system. While processing of *m*-xylene by *upper* pathway enzymes generates intermediates alien to the innate metabolic network of *P. putida*, the final product of the *upper* route 3MBz (Fig. 1) is a faulty substrate of the chromosomally encoded *ortho*-fission pathway, which generates dead-end metabolites (Rojo *et al*., 1987). This possible metabolic misrouting is solved through a regulatory device that ensures that 3MBz induces the plasmid-encoded meta-fission pathway but not the *ortho*-cleavage route encoded by the *ben* and *cat* genes (Perez-Pantoja *et al*., 2014; Silva-Rocha and de Lorenzo, 2014). When cells are grown in toluene, however, the metabolic and regulatory scenario changes, as the action of the *upper* TOL pathway on this aromatic produces benzoate which induces both the *lower* TOL pathway and the chromosomal *ben* genes (Fig. 7). How do these two routes manage their simultaneous action on benzoate? To answer this question, we started by examining expression of TOL plasmid-coded genes when *P. putida* mt-2 is exposed to toluene under the same conditions used before for *m*-xylene. As shown in Fig. 4D, when cells were cultured in succinate-minimal medium and treated with toluene, the gross expression pattern of the *xyl* genes was indistinguishable from that observed before with the *m*-xylene condition (compare Fig. 4D with Fig. 2B): the *upper* and *lower* operons and the *xylS* genes were highly expressed, whereas *xylR* appeared to be downregulated (Fig. 4B). Endogenously produced benzoate was thus inducing the *meta* pathway. When benzoate was instead added as a purified chemical to succinate-grown cells, there was induction only of the *lower* operon (Fig. 4E) but to a lower extent than expression observed with toluene (compare Fig. 4E with Fig. 4D). In this respect, the effects of toluene/benzoate on the regulatory network of the *xyl* genes are virtually indistinguishable of those of *m*-xylene/3MBz. Figure S3

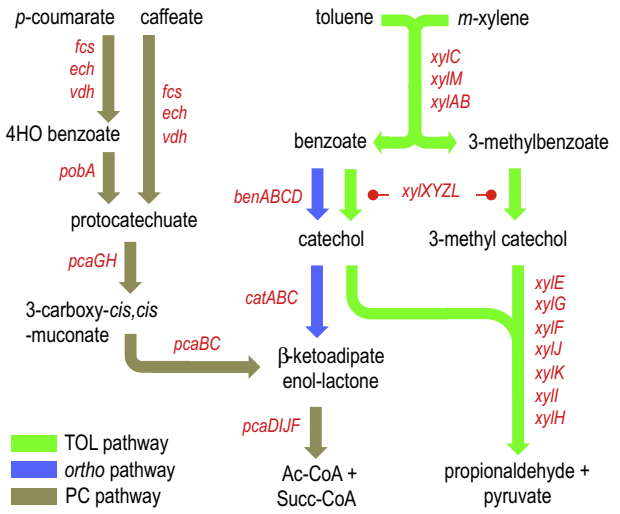

Fig. 7. Aromatic catabolic pathways sharing metabolites in *P. putida* mt-2. Key reactions connected to benzoate and β-ketoadipate catabolism. While the pWW0-encoded meta-cleavage pathway for benzoate degradation is all encoded in the long, polycistronic *meta* operon of the TOL system, the chromosomally determined *ortho* route is composed of non-contiguous *ben*, *cat* and *pca* gene clusters. In *P. putida*, the *pca* genes are themselves scattered over several portions of the chromosome and are organized in three different groupings: *pcaRKFTBDCP*, *pcaIJ* and *pcaGH* (Jimenez *et al.*, 2002). All of the *pca* genes are controlled by the PcaR in *P. putida* PRS2000, except the *pcaT* and *pcaGH* genes (Hughes *et al.*, 1988; Parales and Harwood, 1993; Romero-Steiner *et al.*, 1994; Guo and Houghton, 1999). The connections of the *pca* genes with upstream substrates, e.g. coumarate/4OH-benzoate and caffeate, are indicated.

summarizes the relative responsiveness of each of the transcriptional units that compose the TOL system when *P. putida* mt-2 cells are exposed to pathway head substrates (*m*-xylene, toluene), added intermediates (3MBz and benzoate) and the gratuitous inducer *o*-xylene. Expectedly, the more pronounced differences happen in the *lower* pathway. Yet, expression levels in response to 3MBz and benzoate (whether endogenously produced from head substrates or added to the medium as such) were almost identical – as if the *ortho* route was unable to divert much of the benzoate into this chromosomally encoded pathway. The experiments below allowed us to trace the destiny of benzoate – as compared with 3MBz, when the substrate bifurcates between two different catabolic pathways in this bacterium.

The benzoate biodegradation subtranscriptome of P. putida *mt-2*

Figure 7 sketches the whole of genes known to participate in degradation of *m*-xylene, toluene and their intermediates in *P. putida* mt-2 (Jimenez *et al.*, 2002). On one hand, catechol can be generated from benzoate through the action of both the *m*-toluate dioxygenase encoded by *xylXYZL* genes of pWW0 and the benzoate dioxygenase chromosomally encoded by *benABCD*. On the other hand, once catechol is formed, it can proceed either through the rest of the *meta*-cleavage pathway determined by the single, polycistronic *lower* TOL operon or by the alternative route formed by biochemical activities determined by the independent gene cluster *catABC* and additional enzymes recruited from a separate protocatechuate degradation pathway (*pcaDIJF*; Jimenez *et al.*, 2002). Since these chromosomally encoded routes are independently regulated by pathway substrates and cognate metabolic intermediates, their transcription is a plausible proxy of their biochemical activities.

On this background, we set out to examine with tiling array technology the expression of the *ben*, *cat* and *pca* gene clusters in response to the same panel of inducers than those used for inspection of the *xyl* genes above. Figure 8 shows the results, which embody a considerable amount of information. The control conditions were those of Fig. 8A, in which succinate-grown bacteria were supplied with exogenously added benzoate. The tiling array signals show a considerable induction of the *benABCD* segment (determining the key benzoate dioxygenase activity), *catBCA* and *pcaI* genes and, to a lesser level, the rest of the *ben* (*benKA*$_2$*EF*) and *pca* (*pcaKFTBDC pcaJ*) clusters. Since the signal intensities along the cognate gene sequences are calculated on the basis of the C-runout conditions, comparison of Fig. 8A with Fig. 8B (succinate-grown cells, no other additions) allowed us to discriminate genuine induction by benzoate from default constitutive expression. Under such a criterium, expression of the whole *ben* and *cat* operons seems to be genuinely triggered by benzoate, while that of *pca* genes was generally constitutive or semi-constitutive. No changes were detected either in other connected pathways that share *pca* genes, e.g. coumaric acid, caffeic acid and ferulic acid (Jimenez *et al.*, 2002; Fig. 7). These compounds are channelled towards protocatechuate by enzymes encoded by the *fcs* cluster (*fcs*, *vdh*, *ech* genes) and the *pobA* gene and further taken towards β-ketoadipate by *pca*-encoded products. As shown in Fig. S4, these gene clusters were expressed roughly constitutively regardless of culture conditions. This made us focus our attention on the *ben* and *cat* operons.

As shown in Fig. 8A, *ben* genes appear as a polycistronic operon with at least two differentially stable segments, the most conspicuous being the one encompassing the *benABCD genes*. That the *cat* genes are also induced signifies that at least part of the catechol resulting from the activity of benzoate dioxygenase (or the toluate dioxygenase, see above) has indeed been channelled through the *ortho* route. This is because CatR, the activator of the *cat* cluster, is turned on by *cis-cis* muconate, the product of the *ortho*-ring cleavage (Rothmel *et al.*,

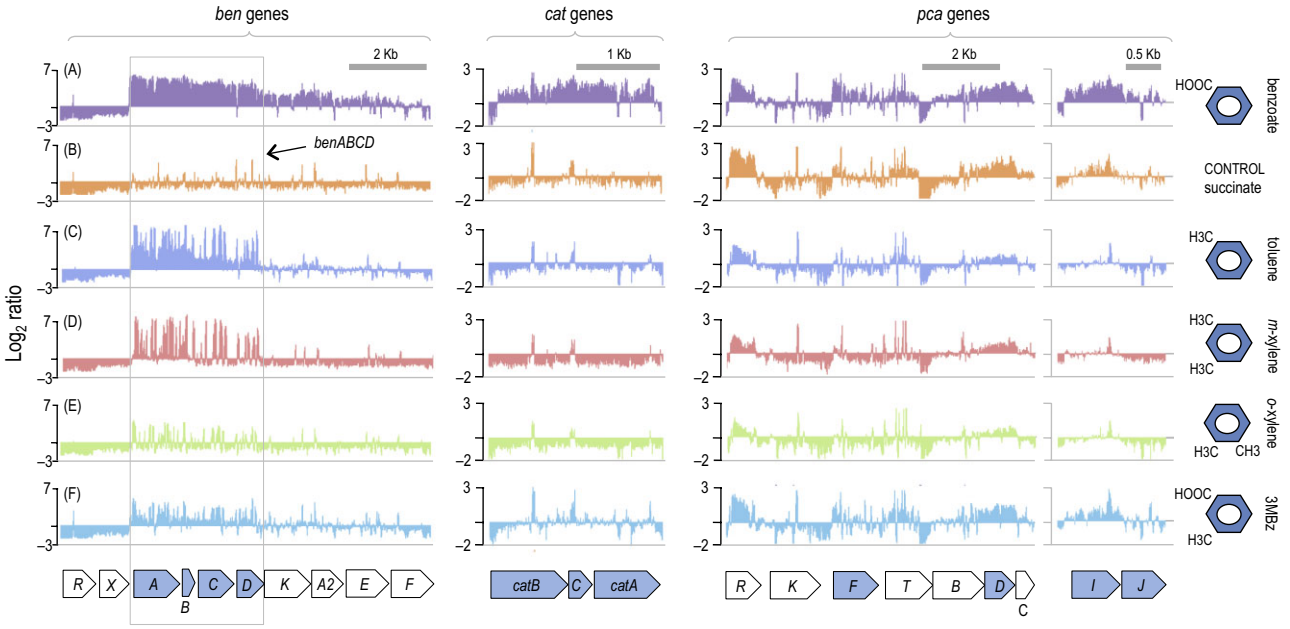

Fig. 8. Expression of *ortho* pathway genes *ben*, *cat* and *pca* in *P. putida* mt-2 exposed to different types of TOL inducers. Transcription profiles were generated with tiling array hybridized with samples from bacteria grown in succinate and added with the inducers indicated: (A) benzoate, (B) control succinate only, (C) toluene, (D) *m*-xylene, (E) *o*-xylene, (F) 3MBz. Signals are normalized in respect to the C-runout condition. Y-axis, Log_2 signal ratio. The *ben*, *cat* and *pca* genes directly involved in benzoate degradation are indicated in light blue. *benABCD* genes are caged for easier comparison.

1991; Schell, 1993; Chugani *et al*., 1998). The fate of the next metabolites of the *cat*-encoded activities (i.e. β-ketoadipate) cannot be predicted so precisely out of the data of Fig. 8A. Yet, the apparent induction of at least gene *pcaI* suggests that degradation of benzoate through the multi-operon *ortho* pathway is likely to proceed to completion.

Taken together, all these data indicate that benzoate added to the medium is split by *P. putida* mt-2 into two separate but compatible (*ortho* and *meta*) degradation routes – although the actual share cannot be determined with this technology.

The metabolic fate of endogenously produced benzoate

The next question was the status of the *ben/cat/pca ortho* pathway transcriptome when benzoate is generated endogenously out of toluene metabolism by the *upper* TOL pathway enzymes (not supplied from outside as before). The results of such a situation are shown in Fig. 8C. Unlike exogenous addition of benzoate (Fig. 8A), we could detect no induction of *benKA$_2$EF*, *catCBA* and *pca* genes. Still, there was a clear signal in the tiling array spanning the *benABCD* sequences. However, unlike the results with benzoate in the same region (Fig. 8A), the level and continuity of the signals through that region were not even, thereby raising the suspicion of artefactual cross-hybridization with the highly similar *xylXYZL* genes of the *lower* TOL pathway (Harayama and Rekik, 1993), which become expressed at high levels in the presence of toluene (Fig. 4D). To clarify this uncertainty, we constructed plasmids bearing transcriptional (P_{benA}→*lacZ*) and translational (P_{benA}→*benA′-′lacZ*) reporter fusions, passed them to *P. putida* mt-2 and measured accumulation of β-galactosidase in the same conditions adopted for RNA extraction. The data shown in Fig. S5 clearly indicated that endogenous benzoate altogether fails to bring about activity of the P_{benA} promoter. Therefore, the tiling array signals coming from *benABCD* in Fig. 8C can be traced to the aforementioned similarity between *benABCD* and *xylXYZL* sequences. The same holds true for the signals in the same region caused by *m*-xylene (Fig. 8D) and *o*-xylene (Fig. 8E) as none of these inducers had significant effect on the activity of the P_{benA}→*lacZ* and P_{benA}→*benA′-′lacZ* fusions (Fig. S5). Finally, 3MBz (Fig. 8F) is known not to be an effector of BenR and also that the complex XylS/3MBz is unable to activate P_{benA} (Perez-Pantoja *et al*., 2014). This reiterates that there is little or no activity of *benABCD* pathway and the other *ortho* pathway clusters in conditions other than external addition of benzoate.

These results tell us that while benzoate is indeed produced out of toluene in *P. putida* mt-2, it is instantly directed to the pWW0-encoded *meta* pathway and not to the chromosomal *ortho* route. This is reflected in the lack of induction of *ben/cat/pca* genes with toluene, as if the chromosomal pathway (unlike the TOL system) could not

see the intracellular benzoate. This may be due to: (i) differences in kinetic and thermodynamic parameters of the enzymes involved that prevent benzoate to accumulate to levels sufficient to activate BenR/P_{benA}, (ii) an active inhibition of *ben/cat/pca* expression by unknown TOL-encoded functions or (iii) a physical channelling (Castellana *et al*., 2014; de Lorenzo *et al*., 2014) of the benzoate coming from the *upper* TOL pathway into the lower enzymatic complex. While these mechanistic questions are beyond the scope of this work, they expose that *P. putida* mt-2 had to evolve some sort of biochemical and/or genetic patch to solve the problem created by the coexistence of two potentially conflicting pathways (Jimenez *et al*., 2014).

Conclusion

The tiling array described in this work for examining the TOL sub-transcriptome has been invaluable to clarify a number of standing questions that could not be addressed before with one-at-a-time approaches that have largely dominated the study of this archetypical metabolic and regulatory network. One key technical choice to this end has been the adoption of the C-runoff samples as the reference condition (Guell *et al*., 2009) for establishing a baseline that allowed us to faithfully compare all other cases. This stratagem exposed: (i) a significant level of basal expression of the *lower* TOL pathway in the absence of inducers (in contrast with virtually no expression of the *upper* route), (ii) the presence of a distinct transcript downstream of the *xylN* gene and (iii) the overlapping transcription between the 3′ ends of the convergent *xylS* and *xylH* mRNAs, a somewhat frequent occurrence in genomes (Hovik *et al*., 2012). Yet, the most surprising finding was that benzoate generated from toluene catabolism by the *upper* pathway failed to induce expression of the *ortho*-cleavage genes. These results are compatible with a hypothetical scenario in which the enzymes of the *upper* pathway could be localized close to the enzymes of the *lower* pathway. In this way, a metabolically produced benzoate could be directly channelled towards the *meta* route. When benzoate is added directly to culture medium, such a channelling effect may disappear and both the *meta* and *ortho* pathway genes can be simultaneously expressed. This hypothetical setting – or any of its alternatives mentioned above, puts some focus on the retroactivity between a pre-existing metabolic chassis and the acquisition of a new biochemical module (Del Vecchio, 2015) whether by naturally occurring horizontal gene transfer or by genetic engineering. Specifically, the data above suggest a range of enzymatic, regulatory (and perhaps physical) devices that work as the *interlocks* of engineered items, i.e. they help prevent the system from damaging itself by interrupting its operation when it meets trouble. Enzymatic misrouting between coexisting pathways is one of the most common of such biochemical conflicts. In previous reports (Jimenez *et al*., 2014; Perez-Pantoja *et al*., 2014), we have identified different metabolic and regulatory devices for avoiding such clashes at various checkpoints of the aromatic biodegradation network of *P. putida* mt-2, and many more are likely to exist (Danchin, 2009). Understanding the mutual adaptation between chassis (e.g. environmental bacteria) and implants (e.g. metabolic pathways found in transmissible plasmids) will be of great value for engineering microbial production of biofuels and added-value chemicals (Kung *et al*., 2012; Nikel and de Lorenzo, 2014; Nikel *et al*., 2014).

Experimental procedures

Strains and growth condition

Unless otherwise indicated, *Escherichia coli* and *P. putida* were routinely grown at 37 and 30°C, respectively, in Luria–Bertani or M9 minimal medium including 6 g l^{-1} Na_2HPO_4, 3 g l^{-1} KH_2PO_4, 1.4 g l^{-1} $(NH_4)_2SO_4$, 0.5 g l^{-1} NaCl, 0.2 g l^{-1} $MgSO_4{\cdot}7H_2O$ and 2.5 ml l^{-1} of a trace element solution as noted (Abril *et al*., 1989; Nikel and de Lorenzo, 2013), with a carbon source as described below. For induction of TOL catabolic genes during transcriptomic experiments, the *P. putida* mt-2 strain was precultured overnight in M9 medium with succinate, and bacterial cultures were then diluted 100-fold in the same medium and grown to the exponential phase (OD_{600} = 0.3–0.5). Samples were then either cultured further without additional substrate or exposed to vaporous *m*-xylene, toluene or *o*-xylene (one-half dilution in dibutyl phthalate, which is a non-effector for TOL genes) in a flask (2 h). For soluble substrates, benzoate (5 mM) or 3MBz (5 mM) was added to the culture medium once growth had reached OD_{600} ~0.3. For the C-runout condition, the cells were cultured for 96 h in succinate-supplemented minimal medium. The antibiotics kanamycin (Km) 50 μg ml^{-1}, ampicillin (Amp) 150 μg ml^{-1}, streptomycin (Sm) 100 μg ml^{-1}, chloramphenicol (Cm) 30 μg ml^{-1} and gentamicin (Gm) 10 μg ml^{-1} were added to bacterial cultures when necessary.

RNA preparation

Cell cultures were transferred to 1/10 sample volume of ice-cold ethanol/phenol solution (5% water-saturated phenol in ethanol) to protect RNA from degradation and harvested by centrifugation (3800 r.p.m., 15 min, 4°C). After supernatant aspiration, pellets were frozen in liquid nitrogen and stored at –80°C until required. Total RNA was extracted by using the miRNeasy kit (Qiagen) with some modifications. The collected pellets were resuspended into 0.3 ml Tris–HCl (pH 7.5) containing 2 mg ml^{-1} lysozyme and incubated (10 min, 37°C). Lysate (0.1 ml) was used according to manufacturer's instructions. RNase-free DNase (Qiagen) treatment was performed during the isolation procedure to eliminate residual DNA and quality was evaluated on a 2100 Bioanalyzer System (Agilent).

High-density tiling array design and analysis

A custom tiling microarray was designed to contain probes corresponding to the complete *xyl* operon of the TOL plasmid, as well as chromosomal genes encoding both branches of β-ketoadipate pathway and peripheral routes such as *fcs* cluster, *pca* genes, *ben* genes and *cat* genes. Oligonucleotide probes were 60 nucleotides long and were designed to be spaced every 10 nt and overlapping 50 nt. Both sense and antisense probes were designed to integrate the same regions and to identify natural antisense RNAs. Microarrays were synthesized by Agilent in the 8 × 15K format using the online tool eArray (https://earray.chem.agilent.com/earray/). Four biological replicates were hybridized independently for each transcriptomic comparison. Total RNA (20 μg each) was retrotranscribed and aminoallyl labelled using the SuperScript Indirect cDNA Labeling System (Invitrogen) and 5-(3-aminoallyl)-2′deoxyuridine-5′-triphosphate (aa-dUTP, Ambion) following manufacturer's protocols. To avoid antisense artefacts from second-strand cDNA during reverse transcription, actinomycin D was added after the denaturing step at 70°C to a final concentration of 6 μg ml^{-1}, as described (Perocchi *et al.*, 2007). For each sample, aminoallyl-labelled cDNA was resuspended in 0.1 M Na_2CO_3 (pH 9.0) and conjugated with Cy3 or Hyper 5 Mono NHS Ester (CyDye™ Post-labelling Reactive Dye Pack, Amersham), following a dye-swap strategy. Samples were purified with MEGAclear (Ambion) following the manufacturer's instructions. Cy3 and Hyper 5 incorporation was measured in a Nanodrop spectrophotometer (Nanodrop Technologies). Probe preparation and hybridizations were performed as described (Two-Color Microarray-Based Prokaryote Analysis, Agilent Technologies). Samples were placed on ice and rapidly loaded onto arrays, hybridized (65°C, 17 h), then washed once in GE Wash Buffer 1 (room temperature, 1 min) and once in GE Wash Buffer 2 (37°C, 1 min). Arrays were drained by centrifugation (2000 r.p.m., 2 min).

Images from Cy3 and Hyper 5 channels were equilibrated and captured with a GenePix 4000B Microarray Scanner (Axon) and spots were quantified using GenePix software (Axon) for tiling array data sets (*m*-xylene versus succinate). For other tiling array data sets that are reference condition-based comparisons, we used the Agilent DNA Microarray Scanner and quantified images using Agilent Feature Extraction software. After scanning and quantification, data from both data sets were analysed using the same methods. Raw intensities were background corrected by the normexp method with an offset of 50 (Smyth and Speed, 2003). Background-corrected intensities were converted to $\log_2$ scale and normalized by adjusting the quantiles of all replicates as described (Bolstad *et al.*, 2003). After normalization, differential expression for each probe was calculated as $\log_2$Ratios = $\log_2$Intensity (experimental condition) – $\log_2$Intensity (control condition). Differential expression at the gene level was calculated by averaging all $\log_2$Ratios of the probes that overlap with the gene coordinates. All statistical calculations were carried out with R software (The Development Core Team, 2011) and the Bioconductor package *limma* (Smyth, 2004). Integrated Genome Browser (IGB) (Nicol *et al.*, 2009) was used to represent the $\log_2$Ratios of all probes in the genomic regions. The Gene Expression Omnibus (GEO, www.ncbi.nlm.nih.gov/geo) accession number for both raw and processed data of the tiling and RNA-seq is GSE71853.

cDNA library construction for RNA deep sequencing

Total RNAs from *m*-xylene-treated cells or reference conditions were prepared. rRNA was depleted using the RiboZero rRNA removal kit (Epicenter Biotechnologies) for Gram-negative bacteria with a total RNA input of 4 μg. To confirm rRNA removal, we analysed the samples with the bioanalyser system as described above. RNA libraries were prepared using the TruSeq RNA sample prep kit (Illumina) following the protocol described in the TruSeq RNA Sample Preparation Guide, starting at the fragmentation step. The library was validated by running a High Sensitivity DNA chip (Agilent Technologies) on the bioanalyser system and quantified by qPCR according to the Illumina Sequencing Library qPCR Quantification Guide using KAPA SYBR FAST qPCR kit for LC480 (KAPA Biosystems). The libraries were denatured and adjusted to 14 pM prior to generating the clusters as indicated in the Illumina Cluster Generation Guide for a Cluster Station instrument. Clusters were generated in one lane of the flow cell, which was sequenced in a single read 1 × 75 bp run by the Genome Analyzer IIx system.

Sequence read alignment and normalization for RNA deep sequencing

Short reads were aligned to the *P. putida* genome and pWW0 plasmid genes with the BWA algorithm with default settings (Li and Durbin, 2009). Mapped counts were normalized by TMM (Robinson and Oshlack, 2010) using the sample whose 75%-ile (of library-scale-scaled counts) is closest to the mean of 75%-iles as the reference. This is the default normalization method when applying the edgeR method (Robinson and Smyth, 2008) for analysing gene expression differences by RNA-seq. After normalization, differential expression was estimated by the method implemented in edgeR software, based on the negative binomial distribution of the reads. For estimating data dispersion, edgeR uses the quantile-adjusted conditional maximum likelihood (qCML) method. In this case, a common dispersion was considered for all samples. The alignment was visualized using the IGV (Thorvaldsdottir *et al.*, 2012).

Preparation of sense strand and antisense strand RNA probes

The *xylS* intergenic region (260 bp) and the non-coding region (170 bp) between *xylS* and *xylH* were amplified by PCR using DNA template from *P. putida* mt-2 with the primer pairs *xylS*nr-F (CGCGCATGCACAATCTCCAGCAACTCGATG)/*xylS*nr-R (CGCGAGCTCC ATCATCGCCAGCTCCGCTAA) and *xylSH*nr-F (CGCGCATGCGAAGGGATGGGTTGGCATCGC)/*xylSH*nr-R (CGCGAGCTCTGAAGTGGAGATCCCAAGGGC). The PCR products were cloned into the pGEM-T-easy vector to generating pGEM-T-*xylS*nr and pGEM-T-*xylSH*nr respectively. To prepare sense RNA

probes, the recombination vectors were *Sac*I digested. After the enzyme reaction, Klenow (NEB) was used to avoid non-specific transcription. For *in vitro* transcription, we used T7 RNA polymerase with ^{32}P-radiolabelled CTP (Promega, Riboprobe combination system). To synthesize antisense RNA probes, *Sph*I enzyme and SP6 RNA polymerase were used with the same procedure as sense RNA probe synthesis. Labelled probes were purified using NICK columns (GE Healthcare).

Northern blot analysis

RNA samples (5 μg) were fractionated on 1% agarose-formaldehyde gels and transferred to membranes (Zeta-Probe, Bio-Rad) by capillary methods (Chomczynski, 1992), and fixed by ultraviolet cross-linking. Membranes were hybridized with ^{32}P-CTP radiolabelled strand-specific sense- and antisense RNA probes for the *xylS* region and the non-coding region between *xylS* and *xylH* in ULTRAhyb ultrasensitive hybridization buffer (Ambion) (68°C, overnight). Membranes were washed twice with 2× SSC (0.1% SDS; 68°C, 15 min) and twice with 0.1× SSC (0.1% SDS) (68°C, 5 min), then exposed to X-ray film.

Cloning procedures and construction of reporter fusions

For both sense and artificial antisense transcriptions of the *xylS*, the 1458 bp fragment from the *xylS* region covering its own promoter (*Ps*) and its extended 3′ end was amplified using primers *xylS*-F (5'CGCTCTAGACTTAAAAAGAACGT CTTCGTT3′) and *xylS*-R (5′CGCGAGCTCGGATGCGCCGC TGACCAGCGT3′). The amplicon was cloned into the XbaI/SacI cloning sites of the pSEVA224 vector (Silva-Rocha *et al.*, 2013) including the LacI^q P*trc* cargo to transcribe *xylS* in the antisense direction, to generate pSEVA224-XS. The plasmid construct was then introduced into *E. coli* CC118 by transformation. The pSEVA224-XS plasmid was then introduced by triparental conjugation into *P. putida* MEG3D harbouring the *Pm* promoter fused to the *gfp-lacZ* reporter gene on chromosome (Silva-Rocha and de Lorenzo, 2012), thus resulting in *P. putida* MEG3D (pSEVA224-XS). To confirm the DNA sequence of the *xylL* gene, its partial region was amplified using the primers xylL-F (5′CGCGCATGCACTTCGAA CACCTCGTAGCC3′)/xylL-R (5′CGCGA GCTCGGTCGAGG CAATTCTGTTCC3′) based on the TOL plasmid in the *P. putida* mt-2 strain as template. Restricting both the PCR product and the pSEVA431 plasmid (Silva-Rocha *et al.*, 2013) with *Sph*I and *Sac*I enzymes, cloning was performed for the partial *xylL* gene and the construct was used to validate the annotated DNA sequence. To generate a transcriptional or a translational fusion of *PbenA* to *lacZ*, the promoter region was amplified using the Pben-F (5′ATGGAGCTC ACCTGGTAGCTGCAAAAGGA3′)/Pben-R (5′GTCGGATCC GCCAGGGTCTCCCTTGTTAT3′) primer pairs or Pben-F/PbenT-R (5′CGCGGATCCGGGTCGGTGAACATC3′), and the PCR product was cloned into pSEVA225 or pSEVA225T (Silva-Rocha *et al.*, 2013) for the transcriptional or translational fusion respectively. Each construct was then transferred into the *P. putida* mt-2 strain by tripartite mating as explained in Martinez-Garcia and de Lorenzo (2012).

Quantification of GFP fluorescence

The strains under examination express a stable GFP variant that absorbs light at 488 nm and GFP activity was normalized as fluorescent unit/OD_{600}. For GFP quantification by flow cytometry, cells cultured overnight were diluted 1:100 in fresh M9-succinate medium and allowed to grow to mid-exponential phase, then divided in new medium with 3MBz (5 mM), 3MBz plus IPTG (1 mM) or no inducer (control). Cultures (500 μL) were sampled at each time point (0, 1 and 2 h) and kept on ice for further analysis. For flow cytometry, samples were loaded in a Gallios Flow Cytometer (Beckman Coulter) and analysed for GFP expression [488/525(40)BP]. For each sample, 15 000 cells were analysed. Results were processed using Kaluza software (Beckman Coulter).

β-galactosidase activity assays

To test the activity of transcription or translation fusion for *PbenA* to *lacZ*, reporter strains were cultured in M9-succinate medium until the exponential phase, inducers were added where appropriate (2 h), and cells were prepared to measure β-galactosidase. Activity was measured with the Galacton-Light Plus system (Applied Biosystems), which is based on a chemiluminescent substrate of the enzyme (Galacton-Plus, Tropix). A sample of cells (500 μl; OD_{600} = 0.3–0.6) was centrifuged (13 000 r.p.m., 1 min, room temperature) and the pellet resuspended in 200 μl of lysis buffer (100 mM potassium phosphate, pH 7.8, 0.2% Triton X-100). The lysis mixture was subjected to two freeze-thaw cycles and centrifuged to eliminate cell debris. Lysed supernatant (20 μl) was incubated (30 min) with 80 μl of reaction buffer (100 mM sodium phosphate, pH 8.0, 1 mM $MgCl_2$, 1X Galacton-Plus). These reactions were performed in 96-well plates and recorded in a luminometer for 30 s immediately after addition of 125 μl of a light emission accelerator (Accelerator-II Sapphire-II) following manufacturer's instructions.

Acknowledgements

The authors are grateful to J.M. Franco (Genomics Unit, CNB) for his help with the design of the tiling array. This work was supported by the CAMBIOS Project of the Spanish Ministry of Economy and Competitiveness, the ST-FLOW, EVOPROG, ARISYS and EMPOWERPUTIDA contracts of the EU and the PROMPT Project of the Autonomous Community of Madrid. The authors declare no conflict of interest

References

Abril, M.A., Michan, C., Timmis, K.N., and Ramos, J.L. (1989) Regulator and enzyme specificities of the TOL plasmid-encoded upper pathway for degradation of aromatic hydrocarbons and expansion of the substrate range of the pathway. *J Bacteriol* **171:** 6782–6790.

Aranda-Olmedo, I., Ramos, J.L., and Marques, S. (2005) Integration of signals through Crc and PtsN in catabolite repression of *Pseudomonas putida* TOL plasmid pWW0. *Appl Environ Microbiol* **71:** 4191–4198.

Assinder, S.J., and Williams, P.A. (1990) The TOL plasmids: determinants of the catabolism of toluene and the xylenes. *Adv Microb Physiol* **31:** 1–69.

Bertoni, G., Marques, S., and de Lorenzo, V. (1998) Activation of the toluene-responsive regulator XylR causes a transcriptional switch between sigma 54 and sigma70 promoters at the divergent *Pr/Ps* region of the TOL plasmid. *Mol Microbiol* **27:** 651–659.

Bolstad, B.M., Irizarry, R.A., Astrand, M., and Speed, T.P. (2003) A comparison of normalization methods for high density oligonucleotide array data based on variance and bias. *Bioinformatics* **19:** 185–193.

Cases, I., Pérez-Martin, J., and de Lorenzo, V. (1999) The IIA^{Ntr} (PtsN) Protein of *Pseudomonas putida* mediates the C source inhibition of the sigma 54-dependent *Pu* promoter of the TOL plasmid. *J Biol Chem* **274:** 15562–15568.

Castellana, M., Wilson, M.Z., Xu, Y., Joshi, P., Cristea, I.M., Rabinowitz, J.D., *et al*. (2014) Enzyme clustering accelerates processing of intermediates through metabolic channeling. *Nat Biotechnol* **32:** 1011–1018.

Chomczynski, P. (1992) One-hour downward alkaline capillary transfer for blotting of DNA and RNA. *Anal Biochem* **201:** 134–139.

Chugani, S.A., Parsek, M.R., and Chakrabarty, A.M. (1998) Transcriptional repression mediated by LysR-type regulator CatR bound at multiple binding sites. *J Bacteriol* **180:** 2367–2372.

Danchin, A. (2009) Cells need safety valves. *Bioessays* **31:** 769–773.

Del Vecchio, D. (2015) Modularity, context-dependence, and insulation in engineered biological circuits. *Trends Biotechnol* **33:** 111–119.

Dominguez-Cuevas, P., Gonzalez-Pastor, J.E., Marques, S., Ramos, J.L., and de Lorenzo, V. (2006) Transcriptional tradeoff between metabolic and stress-response programs in *Pseudomonas putida* KT2440 cells exposed to toluene. *J Biol Chem* **281:** 11981–11991.

Dominguez-Cuevas, P., Marin, P., Marques, S., and Ramos, J.L. (2008) XylS-*Pm* promoter interactions through two helix-turn-helix motifs: identifying XylS residues important for DNA binding and activation. *J Mol Biol* **375:** 59–69.

Dominguez-Cuevas, P., Ramos, J.L., and Marques, S. (2010) Sequential XylS-CTD binding to the *Pm* promoter induces DNA bending prior to activation. *J Bacteriol* **192:** 2682–2690.

Gallegos, M.T., Marques, S., and Ramos, J.L. (1996) Expression of the TOL plasmid xylS gene in Pseudomonas putida occurs from a alpha 70-dependent promoter or from alpha 70- and alpha 54-dependent tandem promoters according to the compound used for growth. *J Bacteriol* **178:** 2356–2361.

Gonzalez-Perez, M.M., Ramos, J.L., and Marques, S. (2004) Cellular XylS levels are a function of transcription of *xylS* from two independent promoters and the differential efficiency of translation of the two mRNAs. *J Bacteriol* **186:** 1898–1901.

Greated, A., Lambertsen, L., Williams, P.A., and Thomas, C.M. (2002) Complete sequence of the IncP-9 TOL plasmid pWW0 from *Pseudomonas putida*. *Environ Microbiol* **4:** 856–871.

Guell, M., van Noort, V., Yus, E., Chen, W.H., Leigh-Bell, J., Michalodimitrakis, K., *et al*. (2009) Transcriptome complexity in a genome-reduced bacterium. *Science* **326:** 1268–1271.

Guo, Z., and Houghton, J.E. (1999) PcaR-mediated activation and repression of *pca* genes from *Pseudomonas putida* are propagated by its binding to both the -35 and the -10 promoter elements. *Mol Microbiol* **32:** 253–263.

Harayama, S., and Rekik, M. (1990) The meta cleavage operon of TOL degradative plasmid pWW0 comprises 13 genes. *Mol Gen Genet* **221:** 113–120.

Harayama, S., and Rekik, M. (1993) Comparison of the nucleotide sequences of the meta-cleavage pathway genes of TOL plasmid pWW0 from *Pseudomonas putida* with other *meta*-cleavage genes suggests that both single and multiple nucleotide substitutions contribute to enzyme evolution. *Mol Gen Genet* **239:** 81–89.

Harayama, S., Lehrbach, P.R., and Timmis, K.N. (1984) Transposon mutagenesis analysis of meta-cleavage pathway operon genes of the TOL plasmid of *Pseudomonas putida* mt-2. *J Bacteriol* **160:** 251–255.

Harayama, S., Rekik, M., Wubbolts, M., Rose, K., Leppik, R.A., and Timmis, K.N. (1989) Characterization of five genes in the upper-pathway operon of TOL plasmid pWW0 from *Pseudomonas putida* and identification of the gene products. *J Bacteriol* **171:** 5048–5055.

Harwood, C.S., and Parales, R.E. (1996) The beta-ketoadipate pathway and the biology of self-identity. *Annu Rev Microbiol* **50:** 553–590.

Holtel, A., Marques, S., Mohler, I., Jakubzik, U., and Timmis, K.N. (1994) Carbon source-dependent inhibition of *xyl* operon expression of the *Pseudomonas putida* TOL plasmid. *J Bacteriol* **176:** 1773–1776.

Hovik, H., Yu, W.H., Olsen, I., and Chen, T. (2012) Comprehensive transcriptome analysis of the periodontopathogenic bacterium *Porphyromonas gingivalis* W83. *J Bacteriol* **194:** 100–114.

Huber, W., Toedling, J., and Steinmetz, L.M. (2006) Transcript mapping with high-density oligonucleotide tiling arrays. *Bioinformatics* **22:** 1963–1970.

Hughes, E.J., Shapiro, M.K., Houghton, J.E., and Ornston, L.N. (1988) Cloning and expression of *pca* genes from *Pseudomonas putida* in *Escherichia coli*. *J Gen Microbiol* **134:** 2877–2887.

Hugouvieux-Cotte-Pattat, N., Kohler, T., Rekik, M., and Harayama, S. (1990) Growth-phase-dependent expression of the *Pseudomonas putida* TOL plasmid pWW0 catabolic genes. *J Bacteriol* **172:** 6651–6660.

Jimenez, J.I., Minambres, B., Garcia, J.L., and Diaz, E. (2002) Genomic analysis of the aromatic catabolic pathways from *Pseudomonas putida* KT2440. *Environ Microbiol* **4:** 824–841.

Jimenez, J.I., Perez-Pantoja, D., Chavarria, M., Diaz, E., and de Lorenzo, V. (2014) A second chromosomal copy of the *catA* gene endows *Pseudomonas putida* mt-2 with an enzymatic safety valve for excess of catechol. *Environ Microbiol* **16:** 1767–1778.

Kim, J., Oliveros, J.C., Nikel, P.I., de Lorenzo, V., and Silva-Rocha, R. (2013) Transcriptomic fingerprinting of *Pseudomonas putida* under alternative physiological regimes. *Environ Microbiol Rep* **5:** 883–891.

Koutinas, M., Lam, M.C., Kiparissides, A., Silva-Rocha, R., Godinho, M., Livingston, A.G., *et al*. (2010) The regulatory logic of *m*-xylene biodegradation by *Pseudomonas putida*

mt-2 exposed by dynamic modelling of the principal node *Ps/Pr* of the TOL plasmid. *Environ Microbiol* **12:** 1705–1718.

Kung, Y., Runguphan, W., and Keasling, J.D. (2012) From fields to fuels: recent advances in the microbial production of biofuels. *ACS Synth Biol* **1:** 498–513.

Li, H., and Durbin, R. (2009) Fast and accurate short read alignment with Burrows-Wheeler transform. *Bioinformatics* **25:** 1754–1760.

de Lorenzo, V., Sekowska, A., and Danchin, A. (2014) Chemical reactivity drives spatiotemporal organisation of bacterial metabolism. *FEMS Microbiol Rev* **39:** 96–119.

Mader, U., Nicolas, P., Richard, H., Bessieres, P., and Aymerich, S. (2011) Comprehensive identification and quantification of microbial transcriptomes by genome-wide unbiased methods. *Curr Opin Biotechnol* **22:** 32–41.

Marques, S., Ramos, J.L., and Timmis, K.N. (1993) Analysis of the mRNA structure of the *Pseudomonas putida* TOL meta fission pathway operon around the transcription initiation point, the *xylTE* and the *xylFJ* regions. *Biochim Biophys Acta* **1216:** 227–236.

Marques, S., Holtel, A., Timmis, K.N., and Ramos, J.L. (1994) Transcriptional induction kinetics from the promoters of the catabolic pathways of TOL plasmid pWW0 of *Pseudomonas putida* for metabolism of aromatics. *J Bacteriol* **176:** 2517–2524.

Marques, S., Manzanera, M., Gonzalez-Perez, M.M., Gallegos, M.T., and Ramos, J.L. (1999) The XylS-dependent *Pm* promoter is transcribed in vivo by RNA polymerase with sigma 32 or sigma 38 depending on the growth phase. *Mol Microbiol* **31:** 1105–1113.

Martinez-Garcia, E., and de Lorenzo, V. (2012) Transposon-based and plasmid-based genetic tools for editing genomes of gram-negative bacteria. *Methods Mol Biol* **813:** 267–283.

Miyakoshi, M., Nishida, H., Shintani, M., Yamane, H., and Nojiri, H. (2009) High-resolution mapping of plasmid transcriptomes in different host bacteria. *BMC Genomics* **10:** 12.

Moreno, R., Fonseca, P., and Rojo, F. (2010) The Crc global regulator inhibits the *Pseudomonas putida* pWW0 toluene/xylene assimilation pathway by repressing the translation of regulatory and structural genes. *J Biol Chem* **285:** 24412–24419.

Nicol, J.W., Helt, G.A., Blanchard, S.G., Jr, Raja, A., and Loraine, A.E. (2009) The Integrated Genome Browser: free software for distribution and exploration of genome-scale datasets. *Bioinformatics* **25:** 2730–2731.

Nikel, P.I., and de Lorenzo, V. (2013) Engineering an anaerobic metabolic regime in *Pseudomonas putida* KT2440 for the anoxic biodegradation of 1,3-dichloroprop-1-ene. *Metab Eng* **15:** 98–112.

Nikel, P.I., and de Lorenzo, V. (2014) Robustness of *Pseudomonas putida* KT2440 as a host for ethanol biosynthesis. *N Biotechnol* **31:** 562–571.

Nikel, P.I., Martinez-Garcia, E., and de Lorenzo, V. (2014) Biotechnological domestication of pseudomonads using synthetic biology. *Nat Rev Microbiol* **12:** 368–379.

Parales, R.E., and Harwood, C.S. (1993) Regulation of the *pcaIJ* genes for aromatic acid degradation in *Pseudomonas putida*. *J Bacteriol* **175:** 5829–5838.

Passalacqua, K.D., Varadarajan, A., Ondov, B.D., Okou, D.T., Zwick, M.E., and Bergman, N.H. (2009) Structure and complexity of a bacterial transcriptome. *J Bacteriol* **191:** 3203–3211.

Perez-Martin, J., and de Lorenzo, V. (1995) The sigma 54-dependent promoter *Ps* of the TOL plasmid of *Pseudomonas putida* requires HU for transcriptional activation in vivo by XylR. *J Bacteriol* **177:** 3758–3763.

Perez-Pantoja, D., Kim, J., Silva-Rocha, R., and de Lorenzo, V. (2014) The differential response of the *Pben* promoter of *Pseudomonas putida* mt-2 to BenR and XylS prevents metabolic conflicts in *m*-xylene biodegradation. *Environ Microbiol* **17:** 64–75.

Perocchi, F., Xu, Z., Clauder-Munster, S., and Steinmetz, L.M. (2007) Antisense artifacts in transcriptome microarray experiments are resolved by actinomycin D. *Nucl Acids Res* **35:** e128.

Ramos, J.L., Marques, S., and Timmis, K.N. (1997) Transcriptional control of the *Pseudomonas* TOL plasmid catabolic operons is achieved through an interplay of host factors and plasmid-encoded regulators. *Annu Rev Microbiol* **51:** 341–373.

Rescalli, E., Saini, S., Bartocci, C., Rychlewski, L., De Lorenzo, V., and Bertoni, G. (2004) Novel physiological modulation of the *Pu* promoter of TOL plasmid: negative regulatory role of the TurA protein of *Pseudomonas putida* in the response to suboptimal growth temperatures. *J Biol Chem* **279:** 7777–7784.

Robinson, M.D., and Oshlack, A. (2010) A scaling normalization method for differential expression analysis of RNA-seq data. *Genome Biol* **11:** R25.

Robinson, M.D., and Smyth, G.K. (2008) Small-sample estimation of negative binomial dispersion, with applications to SAGE data. *Biostatistics* **9:** 321–332.

Rojo, F., Pieper, D.H., Engesser, K.H., Knackmuss, H.J., and Timmis, K.N. (1987) Assemblage of *ortho* cleavage route for simultaneous degradation of chloro- and methylaromatics. *Science* **238:** 1395–1398.

Romero-Steiner, S., Parales, R.E., Harwood, C.S., and Houghton, J.E. (1994) Characterization of the *pcaR* regulatory gene from *Pseudomonas putida*, which is required for the complete degradation of *p*-hydroxybenzoate. *J Bacteriol* **176:** 5771–5779.

Rothmel, R.K., Shinabarger, D.L., Parsek, M.R., Aldrich, T.L., and Chakrabarty, A.M. (1991) Functional analysis of the *Pseudomonas putida* regulatory protein CatR: transcriptional studies and determination of the CatR DNA-binding site by hydroxyl-radical footprinting. *J Bacteriol* **173:** 4717–4724.

Schell, M.A. (1993) Molecular biology of the LysR family of transcriptional regulators. *Annu Rev Microbiol* **47:** 597–626.

Selinger, D.W., Cheung, K.J., Mei, R., Johansson, E.M., Richmond, C.S., Blattner, F.R., *et al.* (2000) RNA expression analysis using a 30 base pair resolution *Escherichia coli* genome array. *Nat Biotechnol* **18:** 1262–1268.

Silva-Rocha, R., and de Lorenzo, V. (2012) A *GFP-lacZ* bicistronic reporter system for promoter analysis in environmental gram-negative bacteria. *PLoS ONE* **7:** e34675.

Silva-Rocha, R., and de Lorenzo, V. (2014) The pWW0 plasmid imposes a stochastic expression regime to the

chromosomal ortho pathway for benzoate metabolism in *Pseudomonas putida*. *FEMS Microbiol Lett* **356:** 176–183.

Silva-Rocha, R., Tamames, J., dos Santos, V.M., and de Lorenzo, V. (2011a) The logicome of environmental bacteria: merging catabolic and regulatory events with Boolean formalisms. *Environ Microbiol* **13:** 2389–2402.

Silva-Rocha, R., de Jong, H., Tamames, J., and de Lorenzo, V. (2011b) The logic layout of the TOL network of *Pseudomonas putida* pWW0 plasmid stems from a metabolic amplifier motif (MAM) that optimizes biodegradation of *m*-xylene. *BMC Syst Biol* **5:** 191.

Silva-Rocha, R., Martinez-Garcia, E., Calles, B., Chavarria, M., Arce-Rodriguez, A., de Las Heras, A., *et al*. (2013) The Standard European Vector Architecture (SEVA): a coherent platform for the analysis and deployment of complex prokaryotic phenotypes. *Nucl Acids Res* **41:** D666–D675.

Smyth, G.K. (2004) Linear models and empirical bayes methods for assessing differential expression in microarray experiments. *Stat Appl Genet Mol Biol* **3:** Article3.

Smyth, G.K., and Speed, T. (2003) Normalization of cDNA microarray data. *Methods* **31:** 265–273.

Sorek, R., and Cossart, P. (2010) Prokaryotic transcriptomics: a new view on regulation, physiology and pathogenicity. *Nat Rev Genet* **11:** 9–16.

The Development Core Team (2011) *R: A Language and Environment for Statistical Computing*. Vienna, Austria: R Foundation for Statistical Computing.

Thomason, M.K., and Storz, G. (2010) Bacterial antisense RNAs: how many are there, and what are they doing? *Annu Rev Genet* **44:** 167–188.

Thorvaldsdottir, H., Robinson, J.T., and Mesirov, J.P. (2012) Integrative Genomics Viewer (IGV): high-performance genomics data visualization and exploration. *Brief Bioinform* **14:** 178–192.

Toledo-Arana, A., Dussurget, O., Nikitas, G., Sesto, N., Guet-Revillet, H., Balestrino, D., *et al*. (2009) The *Listeria* transcriptional landscape from saprophytism to virulence. *Nature* **459:** 950–956.

Velazquez, F., di Bartolo, I., and de Lorenzo, V. (2004) Genetic evidence that catabolites of the Entner-Doudoroff pathway signal C source repression of the sigma 54 *Pu* promoter of *Pseudomonas putida*. *J Bacteriol* **186:** 8267–8275.

Velazquez, F., Parro, V., and de Lorenzo, V. (2005) Inferring the genetic network of *m*-xylene metabolism through expression profiling of the *xyl* genes of *Pseudomonas putida* mt-2. *Mol Microbiol* **57:** 1557–1569.

Vitale, E., Milani, A., Renzi, F., Galli, E., Rescalli, E., de Lorenzo, V., and Bertoni, G. (2008) Transcriptional wiring of the TOL plasmid regulatory network to its host involves the submission of the sigma 54-promoter *Pu* to the response regulator PprA. *Mol Microbiol* **69:** 698–713.

Voss, J.A., Khedairy, H., Baker, R.F., and Benjamin, R.C. (1990) Molecular cloning of the *xylL-xylE* region from the *P. putida* TOL plasmid, pDK1. *SAAS Bull Biochem Biotechnol* **3:** 54–57.

Williams, P.A., Shaw, L.M., Pitt, C.W., and Vrecl, M. (1997) *xylUW*, two genes at the start of the upper pathway operon of TOL plasmid pWW0, appear to play no essential part in determining its catabolic phenotype. *Microbiology* **143:** 101–107.

Worsey, M.J., and Williams, P.A. (1975) Metabolism of toluene and xylenes by *Pseudomonas putida (arvilla)* mt-2: evidence for a new function of the TOL plasmid. *J Bacteriol* **124:** 7–13.

Yoder-Himes, D.R., Chain, P.S., Zhu, Y., Wurtzel, O., Rubin, E.M., Tiedje, J.M., and Sorek, R. (2009) Mapping the Burkholderia cenocepacia niche response via high-throughput sequencing. *Proc Natl Acad Sci USA* **106:** 3976–3981.

Supporting information

Additional Supporting Information may be found in the online version of this article at the publisher's web-site:

Fig. S1. Blow-up of tiling array signals through the 3′ end of the upper TOL operon.

Fig. S2. Correction of sequence annotation on the *xylL* gene in the pWW0 plasmid of *P. putida* mt-2.

Fig. S3. Average intensity of the probes for the *upper* and *lower* operons, and the *xylS* and *xylR* genes in response to different TOL inducers.

Fig. S4. Average intensity of the probes for phenylpropenoid and *p*-hydroxybenzoate catabolic genes in response to different TOL inducers.

Fig. S5. *PbenA* promoter activity in *P. putida* mt-2 in response to TOL inducers.